

1 **Chromatic summation and receptive field properties**
2 **of blue-on and blue-off cells in marmoset lateral**
3 **geniculate nucleus**

4 C.D. Eiber^{a,b,c}, A.N.J. Pietersen^{a,b,c}, N. Zeater^{a,b,c}, S.G. Solomon^{c,d}, P.R. Martin^{a,b,c}
5
6

7 ^a Save Sight Institute, University of Sydney, Sydney, Australia

8 ^b School of Medical Sciences, University of Sydney, Sydney, Australia

9 ^c Australian Research Council Centre of Excellence for Integrative Brain Function, University
10 of Sydney, Australia

11 ^d Department of Experimental Psychology, University College London, United Kingdom

12 email addresses in order: calvin.eiber@sydney.edu.au, alexander.pietersen@sydney.edu.au,
13 natalie.zeater@sydney.edu.au, samuels@physiol.usyd.edu.au,
14 prmartin@physiol.usyd.edu.au.

15 **Corresponding Author:** P. R. Martin, email: prmartin@physiol.usyd.edu.au, phone: +61 2
16 9382 7539, Postal address: Save Sight Institute, 8 Macquarie St, Sydney 2001, Australia.

17 **Running head:** Cone summation in blue-on cells

18 **Key words:** lateral geniculate nucleus, color vision, primate.
19

20 **Abstract**

21 The "blue-on" and "blue-off" receptive fields in retina and dorsal lateral geniculate nucleus
22 (LGN) of diurnal primates combine signals from short-wavelength sensitive (S) cone
23 photoreceptors with signals from medium/long wavelength sensitive (ML) photoreceptors.
24 Three questions about this combination remain unresolved. Firstly, is the combination of S
25 and ML signals in these cells linear or non-linear? Secondly, how does the timing of S and
26 ML inputs to these cells influence their responses? Thirdly, is there spatial antagonism
27 within S and ML subunits of the receptive field of these cells? We measured contrast
28 sensitivity and spatial frequency tuning for four types of drifting sine gratings: S cone
29 isolating, ML cone isolating, achromatic (S + ML), and counterphase chromatic (S – ML), in
30 extracellular recordings from LGN of marmoset monkeys. We found that responses to
31 stimuli which modulate both S and ML cones are well predicted by a linear sum of S and ML
32 signals, followed by a saturating contrast-response relation. Differences in sensitivity and
33 timing (i.e. vector combination) between S and ML inputs are needed to explain the
34 amplitude and phase of responses to achromatic (S + ML) and counterphase chromatic (S –
35 ML) stimuli. Best-fit spatial receptive fields for S and/or ML subunits in most cells (> 80%)
36 required antagonistic surrounds, usually in the S subunit. The surrounds were however
37 generally weak and had little influence on spatial tuning. The sensitivity and size of S and ML
38 subunits were correlated on a cell-by-cell basis, adding to evidence that blue-on and
39 blue-off receptive fields are specialised to signal chromatic but not spatial contrast.

40

41 **Introduction**

42 Color vision in primates originates in short- (S), medium- (M), and long-wavelength
43 sensitive (L) cone photoreceptors in the retina. The cone signals are processed within the
44 retina to form wavelength-selective afferent channels, including M – L opponent or
45 "red/green" channels, in which M and L signals are differenced, and "blue/yellow" channels,
46 driven by S cones in opposition to combinations of M and L cones. This paper addresses
47 three outstanding questions about S-cone signalling in "blue-on/yellow off" (also known as
48 blue-on, or more properly S-on) cells, and less commonly encountered "blue-off/yellow-on"
49 (also known as blue-off, or more properly S-off) cells. Firstly, is the combination of S and ML
50 signals in these cells linear or non-linear? Secondly, how does the timing of S and ML inputs
51 to these cells influence their responses? Thirdly, is there spatial antagonism within S and ML
52 subunits of the receptive field of these cells? Answers to these questions will improve our
53 understanding of subcortical signals serving color vision.

54 Blue-on and blue-off cells have been the subject of longstanding study (reviewed by
55 Dacey, 2004; Martin & Lee, 2014), and recordings from dorsal lateral geniculate nucleus
56 (LGN) have associated blue-on and blue-off cells with the koniocellular layers of the LGN
57 (Martin, White, Goodchild, Wilder & Sefton, 1997; Roy, Martin, Dreher, Saalman, Hu &
58 Vidyasagar, 2009). The small bistratified (SBS) retinal ganglion cell is established as
59 exhibiting a blue-on/yellow off receptive field (Dacey & Lee, 1994; Szmajda, Martin &
60 Grünert, 2008; Crook, Davenport, Peterson, Packer, Detwiler & Dacey, 2009) but the
61 anatomical substrate of blue-off cells in retina is less clear (reviewed by Dacey, 2004; Martin
62 & Lee, 2014).

63 Firing rates of blue-on cells and blue-off cells are determined by opponent

64 (antagonistic) combination of the S and ML inputs to the receptive field (Yeh, Lee &
65 Kremers, 1995a; Solomon, Lee, White, Rüttiger & Martin, 2005; Field et al., 2007; Tailby,
66 Solomon & Lennie, 2008a; Crook et al., 2009). Responses to stimuli which modulate both S
67 and ML cones should therefore be determined by the (signed) sum of the contrast delivered
68 to the S and ML cones. This prediction was confirmed for blue-on cells in macaque retina
69 when tested using combinations of S and ML contrast in spatially uniform fields (Crook et
70 al., 2009). The question as to whether this finding holds across the spatial frequency tuning
71 range of blue-on and blue-off cells has however not been specifically tested. Further, most
72 ganglion cells, including blue-on and blue-off cells (Yeh et al., 1995a), show some degree of
73 response saturation for high contrast stimuli (Shapley & Victor, 1978; Lee, Virsu & Elepfandt,
74 1983; Kaplan & Shapley, 1986; Solomon et al., 2005) The specific question as to whether
75 response saturation influences responses of blue-on and blue-off cells to combined S and
76 ML contrast has also not been addressed.

77 Lee, Valberg and colleagues showed linear combination of saturating cone inputs can
78 account for responses of blue-on ganglion cells to high-intensity narrow-band lights (Lee et
79 al., 1983; Lee, Valberg, Tigwell & Tryti, 1987). In their model, illustrated schematically in
80 Figure 1, nonlinearities in contrast response are present in the S cone and ML cone signals
81 prior to their combination (Lee et al., 1983; Schnapf, Nunn, Meister & Baylor, 1990). If this is
82 the case, then differences in gain and/or saturation between S and ML inputs could yield
83 non-monotonic "supersaturating" responses to stimuli which activate both inputs. An
84 alternative (but not mutually exclusive) possibility is that linear S cone and ML cone inputs
85 may be first summed, then subject to nonlinear distortion. In this case, the integrated
86 output must be monotonic with increasing contrast. These alternative models were not

87 explicitly compared in previous studies of cone inputs to macaque LGN cells (Lee et al.,
88 1983; Lee et al., 1987). Therefore, the first question we address in this paper is: how linear is
89 cone summation in blue-on and blue-off cells?

90 In addition to assuming linear combination of S and M inputs, most studies among
91 those cited above had assumed that the opponent inputs arrive at the same time at the
92 integrating site, and therefore can be modelled as a simple difference of the input functions.
93 More recent studies, however, indicate that there is a variable degree of delay between S
94 and ML inputs (~5 – 10 ms) to blue-on cells (Chichilnisky & Baylor, 1999; Field et al., 2007;
95 Tailby et al., 2008a; Pietersen, Cheong, Solomon, Tailby & Martin, 2014). Such delays could
96 help account for direction-selective achromatic responses observed in blue-on cells in
97 macaque and marmoset LGN (Tailby et al., 2008a; Tailby, Dobbie, Hashemi-Nezhad, Forte &
98 Martin, 2010), but responses to combined S and ML contrast have not been systematically
99 analysed. This is the second question we address in this paper.

100 The spatial distribution of cone inputs to S cone-signaling cells in the LGN was first
101 described as “Type II”, consisting of spatially overlapping S and ML subfields, in early work
102 by Wiesel and Hubel (1966). Later measurements showed that the ML-off subfield is slightly
103 larger than the S-on subfield (Solomon et al., 2005; Field et al., 2007; Crook et al., 2009).
104 Crook et al. (2009) additionally provide evidence that inputs to the S-on subfield to blue-on
105 SBS cells have centre-surround structure (S-on, ML-off), and blue-on cells showing
106 band-pass response to S cone gratings have been recorded in macaque and marmoset LGN
107 (Tailby et al., 2008a; Tailby, Szmajda, Buzás, Lee & Martin, 2008b). A population survey of
108 the spatial transfer properties of S cone and ML cone receptive field subunits has not been
109 made, and the degree to which blue-on and blue-off cells are specialised to transmit

110 chromatic *versus* spatial signals remains uncertain. Therefore, the third question we address
111 in this paper is: are blue-on cells really Type II cells?

112 **Methods**

113 *Ethical approval.*

114 Procedures conformed to the Australian National Health and Medical Research Council
115 (NHMRC) code of practice for the use and care of animals and institutional animal care and
116 ethics committee at the University of Sydney. Procedures also conform to the code of ethics
117 of the World Medical Association (Declaration of Helsinki).

118 *Animal preparation.*

119 Details of our animal preparation, recording technique, and visual stimulation environment
120 have been published previously (Tailby et al., 2010; Pietersen et al., 2014). To summarize,
121 extracellular recordings of single units were performed in the lateral geniculate nucleus
122 (LGN) of common marmosets *Callithrix jacchus*. Animals were sedated with an
123 intramuscular injection of Alfaxan (12 mg kg⁻¹, Jurox, NSW, AUS) and Diazepam (3 mg kg⁻¹,
124 Roche, NSW, AUS), and anesthesia was maintained by continuous intravenous delivery of
125 Sufentanil citrate (6 – 30 µg kg⁻¹ h⁻¹; Sufenta Forte, Janssen Cilag, Beerse, BEL). Depth of
126 anesthesia was monitored by continuous electroencephalography and pulse oximetry
127 (SurgiVet, OH, USA). The animal was artificially respired with a 70%–30% mixture of
128 NO₂–Carbogen (5% CO₂ in O₂) and head-fixed in a stereotaxic frame. A durotomy was made
129 above the LGN and a guide tube containing the recording electrode was inserted into the
130 brain. Action potential waveforms of single cells were discriminated by principal component
131 analysis of amplified voltage signals from single microelectrodes (5 – 11 MΩ, FHC Inc.,

132 Bowdoin, Maine, USA). The position of each cell relative to the brain surface was recorded
133 from a hydraulic microdrive (David Kopf Model 640). Electrolytic lesions (3–6 $\mu\text{A} \times 3\text{--}6 \text{ s}$,
134 electrode positive) were made to assist in track reconstruction. At the conclusion of
135 recordings the animal was killed with an overdose of pentobarbitone sodium (80–150 mg
136 kg^{-1} , i.v.). The position of recorded cells was reconstructed histologically as described in
137 detail in our previous publications (White, Goodchild, Wilder, Sefton & Martin, 1998;
138 Cheong, Tailby, Solomon & Martin, 2013).

139 *Visual Stimuli*

140 Stimuli comprised drifting sine gratings and sine-modulated flashing dots, displayed on a
141 stimulus monitor (refresh rate 100 or 120 Hz) against a grey background (mean luminance
142 50 cd/m^2) which was centred on each receptive field using a front-silvered gimbaled mirror.
143 The driving voltage of the red, green, and blue phosphors of the stimulus monitor were
144 adjusted to produce cone selective (“silent substitution”) gratings, using the spectral
145 radiance distribution of the monitor phosphors, the sensitivity distribution of the marmoset
146 cone photoreceptors, and knowledge of the spectral absorbance of the optic media and
147 macular pigment (Brainard, 1996; Blessing, Solomon, Hashemi-Nezhad, Morris & Martin,
148 2004; Tailby et al., 2008a). Visual stimuli were generated using custom software which also
149 collected and sorted recorded spike waveforms and times to within 0.1 ms. (EXPO;
150 P. Lennie, University of Rochester, Rochester, NY). The S cone selective stimulus produced
151 60-80% contrast in S cones and less than 5% contrast in ML cones. The ML cone selective
152 stimulus produced 60-80% contrast in ML-class cones and less than 5% contrast in S cones,
153 relative to the nominal maximum achievable Michelson contrast of 100% for an achromatic
154 (S + ML) stimulus, which modulated both cone classes equally. For brevity, the

155 cone-isolating stimuli are referred to as S cone and ML cone stimuli hereinafter. An
156 “optimal” mixed (S – ML) stimulus which drove the S and ML cones in counter-phase at half
157 the RMS cone contrast of the S cone and ML cone stimuli was also used. Drifting gratings
158 typically had a temporal frequency of 5 Hz (range 2-15 Hz). Stimulus aperture was typically
159 4° (range 1° – 12°), adjusted to ensure stimulation of both centre and surround.

160 Spatial frequency tuning curves were collected with drifting gratings ranging from
161 0.1 – 12.8 cycles/degree (cyc/deg) at 50% contrast. Contrast response curves were collected
162 with drifting gratings ranging from 2% – 70% contrast relative to the maximum achievable
163 achromatic contrast, typically at the identified peak spatial frequency (range 0 – 2.7
164 cyc/degree). The amplitude and phase of the first Fourier harmonic of the stimulus
165 frequency were taken as the primary measure of the cells’ response to stimulation.

166 *Analysis of contrast sensitivity*

167 For the purposes of comparing S, ML, S + ML, and S – ML contrast response functions, the
168 amplitude of the cell’s response as a function of contrast were fit to saturating hyperbolic
169 functions (Naka & Rushton, 1966; Sclar, Maunsell & Lennie, 1990) of the form

$$170 \quad K = \frac{M(c^n)}{c^n + c_{50}^n} + b \quad (\text{Eq. 1})$$

171 In which the spike rate K is a function of stimulus contrast c , theoretical maximum spike
172 rate M , semisaturation contrast c_{50} , exponent n , and noise-derived discharge at zero
173 contrast b . The semisaturation contrast c_{50} is the contrast at which the response is at half
174 of maximum. The exponent term n controls the steepness and curvature of the curve at
175 intermediate contrasts. Fits were performed in MATLAB (Mathworks, Natick MA) using
176 constrained non-linear least-squares minimization in which all values were constrained to

177 be positive, the values of c_{50} were constrained to fall between 0 and 200%, and the values
 178 of the exponent term were constrained to be less than 3. These constraints ensured that the
 179 gain of the cell can be estimated even for low amplitude responses. When the fitted
 180 semisaturation constant was greater than the maximum contrast, it indicated a
 181 non-saturating response; when semisaturation constants were not constrained they could
 182 grow without bound without substantially improving the model fit to the data. The contrast
 183 gain is given by the derivative of Eq. 1,

$$184 \quad K' = \frac{n M c^n c_{50}^n}{c(c^n + c_{50}^n)^2} \text{ (Eq. 2)}$$

185 and is computed at the semisaturation point c_{50} for saturating cells ($c_{50} < 100\%$) and at
 186 maximum contrast for non-saturating cells. In prior work where the value of n was fixed
 187 to 1 (e.g. Kaplan and Shapley, 1986), the contrast gain was instead computed at low
 188 contrast ($c = 0$). It can be determined from Eq. 2 that at $c = 0$, K' exists and is non-zero
 189 if and only if $n = 1$.

190 For the purpose of model identification, data were also fit to a simpler version of
 191 Eq. 1 in which the exponent was fixed at 1, and to an elaborated version of Eq. 1. (Peirce,
 192 2007) which permits non-monotonic supersaturating responses:

$$193 \quad K = \frac{M(c^{n_1})}{c^{n_2} + c_{50}^{n_2}} + b. \text{ (Eq. 3)}$$

194 In this model there are two exponent terms n_1 and n_2 , and variables are otherwise as
 195 Eq. 1. To test the hypothesis that this equation with its increased number of free
 196 parameters provided a significantly better fit to the data, we calculated the residual errors
 197 for each model, following Buzás, Kóbor, Petykó, Telkes, Martin & Lénárd (2013). If the more
 198 complex model significantly reduced the residual error over its predecessor, as assessed by

199 a 1-sided 2-sample F test for equal variances ($p < 0.05$), then the more complex model was
 200 adopted. The data were also fit to a model which implements a thresholding rather than an
 201 expansive nonlinearity:

$$K = \max\left(\frac{M(c - c_0)}{c - c_0 + c_{50}}, 0\right) + b. \text{ (Eq.4)}$$

202 In this model the exponent term is fixed to 1, but a constant value is added to the contrast.
 203 At contrasts below c_0 , the predicted response is the noise-derived discharge at zero
 204 contrast b .

205 *Analysis of chromatic summation*

206 Two extended models incorporating alternate hypothetical mechanisms for the
 207 summation of S and ML inputs were fit to the amplitude and phase of each cell's responses.
 208 The first model, illustrated in Figure 1A, assumes separable contrast mechanisms for S cone
 209 and ML cone input and is given by

$$K = \frac{M_S c_S |c_S|^{n_S-1}}{|c_S|^{n_S} + c_{S,50}^{n_S}} + \frac{M_{ML} c_{ML} |c_{ML}|^{n_{ML}-1}}{|c_{ML}|^{n_{ML}} + c_{ML,50}^{n_{ML}}} + b \text{ (Eq. 5)}$$

210 In which K is the complex spike rate, c_S is S cone contrast and phase, M_S is the
 211 theoretical saturation spike-rate (and relative phase) for S cone contrast, n_S is the
 212 exponent of the S cone contrast function, and $c_{S,50}$ is the semisaturation contrast for the S
 213 cone contrast function. The notation for ML cone contrast mirrors that for S cone contrast.
 214 The complex spike rate K is the complex sum of one Naka-Rushton curve representing S
 215 cone input c_S and a second Naka-Rushton curve representing ML cone input c_{ML} . Prior
 216 evidence (Yeh et al., 1995a; Solomon & Lennie, 2005) suggests that phase advance is not
 217 prominent for blue-on cells, and so this expression ignores the phenomenon of phase

218 advance (Shapley & Victor, 1978; Benardete & Kaplan, 1999). In other words, all responses
 219 to S cone stimuli share a single phase, as do all responses for ML cone stimuli. This model
 220 assumes that the nonlinearities in the contrast response are present in the S and ML signals
 221 prior to their combination, and also predicts that the overall contrast response to stimuli
 222 having both S and ML contrasts need not be monotonic where there is a mismatch between
 223 S and ML parameters.

224 An alternative model, illustrated in Figure 1B, assumes linear summation of cone
 225 inputs followed by nonlinear distortion, and is given by

$$K = \frac{(M x)|x|^{(n-1)}}{(|x|^n + c_{50}^n)} + b,$$

$$x = w c_{ML} e^{i\phi_{ML}} + (1 - w)c_S e^{i\phi_S}$$

226 In which the complex spike-rate K is a function of the complex drive x , which itself is the
 227 weighted complex sum of the S cone and ML cone contrasts. As in Eq. 1, M is theoretical
 228 saturation spike-rate, c_{50} is semisaturation contrast, n is an exponent term, and the tonic
 229 discharge rate is b . The ML cone fraction w varies from 1 when the cell receives
 230 exclusively ML cone input to 0 when the cell receives exclusively S cone input, and the
 231 response phase of the S cone and ML cone inputs are given by ϕ_{ML} and ϕ_S , respectively,
 232 for S cone contrast c_S and ML cone contrast c_{ML} . This model assumes that a linear
 233 summation of approximately linear S cone and ML cone signals occurs, and that the output
 234 of that summation is distorted by nonlinearity either at the ganglion cell level, at the
 235 ganglion cell to LGN synapse, or at the point of spike generation in the LGN.

236 *Analysis of spatial distribution of cone inputs*

237 We employed a straightforward extension of the standard difference-of-Gaussians (DoG)
 238 model of Rodieck & Stone (1965) and Enroth-Cugell & Robson (1966), which accounts for
 239 response phase by taking the complex sum of Gaussian kernels (Frishman, Freeman, Troy,
 240 Schweitzer-Tong & Enroth-Cugell, 1987). Each kernel G_n is given by

$$G_n(\omega) = \pi r_n^2 e^{2\pi i(\phi_n + \delta_n \omega) - (\pi r_n \omega)^2} \text{ (Eq. 7)}$$

241 in which the stimulus spatial frequency is ω , the radius of the Gaussian kernel is r_n , the
 242 displacement of the field from the origin is δ_n , and the response phase to a spatially
 243 uniform stimulus is ϕ_n , which is determined from the cell's dominant (S or ML) input and
 244 response latency. The overall response spike-rate K is the complex sum of a variable
 245 number of Gaussian kernels, each having a magnitude M_n ,

$$K = \sum_{n=1}^N M_n G_n(\omega). \text{ (Eq. 8)}$$

246 This formulation is able to support spatial-frequency-dependent changes in response phase
 247 (Enroth-Cugell, Robson, Schweitzer-Tong & Watson, 1983). Fits were performed in MATLAB
 248 again using a constrained non-linear least-squares algorithm. The volume V_n of a receptive
 249 subfield, assuming circular receptive fields (but see also Chichilnisky & Baylor, 1999; Field et
 250 al., 2007; Tailby et al., 2010), is given by

$$V_n = \pi r_n^2 M_n, \text{ (Eq. 9)}$$

251 and can be thought of as the expected response of the cell if all other excitatory or
 252 inhibitory subfields were blocked and the entire subfield were to be stimulated by its
 253 preferred stimulus.

254 Not every cell for which spatial frequency tuning was available also had chromatic contrast
 255 response data, and so in the spatial model contrast nonlinearities are ignored; instead,

256 response amplitudes were normalized by contrast. For each cell, a sequence of
 257 progressively more elaborate models was fit, as described in Table 1.

Model Type	N =	Constraints	Free parameters
Classic type II RF	2 (S,ML)	$r_S = r_{ML}; \delta_S = \delta_{ML};$ $\delta_n < 2 r_n$	6
Simple Opponent Cell	2 (S,ML)	$\delta_n < 2 r_n$	8
S cone Centre-Surround	3 (Sc, Ss, ML)	$r_{Sc} < r_{Ss}; \delta_{Sc} = \delta_{Ss};$ $\phi_{Sc} = \phi_{Ss} + \pi; \delta_n < 2 r_n$	10
ML cone Centre-Surround	3 (S,MLc,MLs)	$r_{MLc} < r_{MLs}; \delta_{MLc} = \delta_{MLs};$ $\phi_{MLc} = \phi_{MLs} + \pi; \delta_n$ $< 2 r_n$	10
Double-Opponent Centre-Surround	4 (Sc, Ss, MLc, MLs)	$r_{Sc} < r_{Ss}; \delta_{Sc} = \delta_{Ss};$ $r_{MLc} < r_{MLs}; \delta_{MLc} = \delta_{MLs};$ $\phi_{Sc} = \phi_{Ss} + \pi;$ $\phi_{MLc} = \phi_{MLs} + \pi;$ $\delta_n < 2 r_n$	12

258

259 For each model, residual errors were calculated and compared using 1-sided 2-sample F
 260 tests for equal variances ($p < 0.1$). The simplest model which significantly reduced the
 261 variance of the data compared to its predecessor was adopted, as described above for
 262 contrast responses.

263 *Dataset*

264 The dataset comprised recordings from 155 cells (51 blue-on cells, 6 blue-off cells, 74 P cells
 265 and 24 M cells) from 27 animals. Responses of 68 cells to parts of the stimulus set were
 266 previously described (Tailby et al., 2008b; Tailby et al., 2010; Pietersen et al., 2014; Cheong
 267 & Pietersen, 2014). What is new here is our analyses of datasets comprising responses to
 268 ML isolating stimuli and mixed chromatic (S – ML) stimuli as well as S and achromatic (S +
 269 ML) stimuli. Most receptive fields (63.3%) were located between 2° and 12° eccentricity;
 270 14.8% were located within 2° of the fovea and 21.9% were located at more than 12°

271 eccentricity. No systematic differences in responses to S cone stimulation were found
272 between trichromatic female animals (identified by the presence of red-green opponent
273 parvocellular cells), and the other dichromatic animals, all of which had a visual phenotype
274 consistent with the presence of S cones and one cone type with peak sensitivity close to 543
275 nm, 556 nm, or 563 nm (ML cones), and so data were pooled for analysis. Not every cell had
276 both a contrast and a spatial frequency measurement recorded.

277 Cells were classified as blue-on, blue-off, parvocellular (P), or magnocellular (M) by
278 the response to brief (200 or 500 ms) temporal square-wave stimuli (Pietersen et al., 2014)
279 supplemented by measurements of spatial and temporal frequency sensitivity. Examples of
280 a typical blue-on, P, and M response are shown in Figure 2.

281 Anatomical locations of 41%, or 64/155 cells (22/51 blue-on, 2/6 blue-off, 32/74 P,
282 and 8/24 M) were confirmed offline with histology as described above. In cases where track
283 location was not determined, the receptive field properties, eye dominance, encounter
284 position, and response characteristics were used as criteria. Based on the combined
285 anatomical and physiological criteria, one blue-on cell was located in the (ventral-most)
286 koniocellular layer K1, 1 cell was in K2 (between the M layers), 17 cells were in K3 (between
287 the M and P layers), 9 were in K4 (between the internal and external parvocellular layers),
288 and 4 cells were in K6 (dorsal to the external parvocellular layer). One blue-on cell was
289 located 'ectopically' in the ipsilateral M layer. The laminar location of 18 blue-on cells could
290 not be determined unequivocally. Two blue-off cells were located in K3, two blue-off cells
291 were located 'ectopically' in a P layer, and two blue-off cell locations could not be
292 determined unequivocally. No systematic differences in blue-on or blue-off cell properties
293 were apparent on comparing receptive fields from different layers.

294 **Results**

295 *Chromatic contrast response functions*

296 Figure 3A shows raster plots of a typical blue-on cell for 2 s presentations of 5 Hz S cone, ML
297 cone, achromatic (S + ML) and mixed chromatic (S – ML) drifting gratings, arranged by
298 stimulus contrast. At intermediate and high contrast the cell clearly responds in a
299 phase-locked manner to each stimulus cycle, and the S cone response appears at close to
300 opposite phase of the ML response. Response phase for S cone and ML cone remains
301 constant across contrast. The lack of contrast-dependent phase advance agrees with
302 previous data from blue-on cells in LGN of macaque and marmoset (Solomon & Lennie,
303 2005; Tailby et al., 2008b) and retina of macaque (Yeh et al., 1995a) and capuchin monkey
304 *Cebus apella* (Silveira et al., 1999). The cell responds only feebly to achromatic (S + ML)
305 stimulus, but responds vigorously to the chromatic (S – ML) stimulus. Figure 3B shows the
306 average firing rate and first 5 Fourier components of the response at maximum contrast; the
307 zeroth and first harmonic contain the majority of the response power. The power in the
308 higher harmonics chiefly arises from rectification of the response; when rectification is
309 addressed by fitting a rectified sine wave to the response, the residual harmonic distortion
310 ratio (HDR; the ratio of the sum of the squares of the 2nd-5th harmonics to the square of the
311 fundamental) decreased by more than 20-fold. Across the population of recoded blue-on
312 cells, correcting for rectification in the response results on average in an 8-fold decrease in
313 HDR (data not shown). Before correcting for rectification, median values of HDR for blue-on
314 cells are 0.57 (90% range 0.13-3.2) for S responses and 0.46 (90% range 0.12-2.0) for ML
315 responses. After correction, these ranges decrease to 0.17 (90% range 0.02-0.88) and 0.16
316 (90% range 0.01-1.04), respectively.

317 Figure 3C shows the amplitude of the first-harmonic responses with fitted
318 Naka-Rushton curves, as given by Eq. 1. The response to S cone stimulation is expansive at
319 low contrast and shows mild saturation at high contrast, yielding a sigmoid shape. Expansive
320 nonlinearity at low contrast is less evident in the off-phase response to ML cone stimulation
321 (Fig. 3B), but are also evident for the response to a mixed chromatic stimulus. It is
322 interesting to note that blue-on ganglion cells in macaque retina show little sign of
323 expansive nonlinearity (Yeh et al., 1995a; Crook et al., 2009); we return to this point in a
324 later section.

325 Figure 3D shows the responses plotted in the complex plane, with time passing in
326 clockwise direction. Plotting the data this way reveals that the ML cone response is in
327 close-to-opposite phase but ~ 10 deg (~ 5 ms at 5 Hz) slower than the S response, as
328 previously reported (Tailby et al., 2010; Pietersen et al., 2014). Figure 3E-H show example
329 responses for a blue-off, yellow-on cell. This cell has a lower baseline firing rate and overall
330 activity, but clear phase-locking and opposite-phase responses can also be observed. The S-
331 and ML cone response phases are opposite to those observed for the blue-on cell.

332 For blue-on cells, there were no significant differences between the distributions of
333 the fitted Naka-Rushton semisaturation constants for curves fitted to the first-harmonic
334 response, as compared to curves fitted to a rectification-corrected harmonic response, for
335 either S, ML, achromatic, or mixed S – ML stimulation ($p > 0.6$ for each case, paired
336 Wilcoxon test). All values reported above were fitted to unmodified first-harmonic
337 responses, as is typically reported. Figure 4 shows distributions of the fitted semisaturation
338 constants (Fig. 4A), maximum gains (Fig. 4C), and exponent parameters (Fig. 4E) fitted using
339 Eq. 1 to S cone and ML cone stimuli for blue-on and blue-off cells, as well as the

340 distributions of these fitted parameters for P and M cells (Fig. 4B, D, and F). Summary
 341 statistics for the data shown in Figure 4 are given in Table 2. As expected (Kaplan & Shapley,
 342 1986; Yeh et al., 1995b), the M cell semisaturation constants were lower, and M cell gain
 343 was significantly higher, than those of P or blue-on cells ($p < 0.01$ for all comparisons, 3-way
 344 Kruskal-Wallis test [KW]). The P cell exponent terms were significantly lower than those of
 345 blue-on or M cells ($p < 0.01$, KW). For blue-on cells, S cone gain was correlated with ML cone
 346 gain (Fig. 4C, $r = 0.77$, $p < 0.01$) and significantly greater than ML gain ($p = 0.01$, 2-way KW),
 347 suiting these cells' description as blue-on as opposed to yellow-off. Similarly, semisaturation
 348 constants fitted to S cone responses were significantly lower than those fit to ML cone
 349 responses ($p < 0.01$, 2-way KW). Of the 33 blue-on cells within 10° of the fovea for which a
 350 contrast response function could be fit, 26 had a clear half-maximal response nonlinearity
 351 ($c_{50} < 100\%$) in their S response and 20 had a clear nonlinearity in their ML response.

352 Table 2

	Semisaturation (%)	Contrast gain (imp/s % ⁻¹)	Exponent
Blue-on cells S cone	63.4 ± 45.2	0.60 ± 0.42	2.4 ± 0.6
Blue-on cells ML cone	87.3 ± 46.7	0.40 ± 0.30	2.3 ± 0.7
Blue-off cells S cone	29.4 ± 17.9	0.55 ± 0.36	2.3 ± 0.8
Blue-off cells ML cone	65.6 ± 58.5	0.32 ± 0.22	2.2 ± 1.0
P cells	92.9 ± 51.0	0.35 ± 0.34	1.9 ± 0.7
M cells	22.1 ± 29.6	2.17 ± 1.34	2.4 ± 0.6

353 All reported values mean ± standard deviation

354 The scatterplot in Figure 4A raises the impression of two populations of blue-on cells with
 355 respectively high and intermediate semisaturation constants. We found however that (apart
 356 from the correlation of S and ML gain noted above) the joint distributions of the fitted
 357 Naka-Rushton parameters for blue-on cells did not hold significant correlations, nor was
 358 there evidence of clustering in the parameter space (data not shown). A low semisaturation

359 constant for S cone contrast neither predicted nor was predicted by a low semisaturation
360 constant for ML cone contrast ($\chi^2 = 0.04$, $p = 0.833$). Contrast gain was mildly correlated
361 with eccentricity for both S cone and ML cone ($r = 0.49$ and $r = 0.55$, respectively); however,
362 no other parameter was correlated with eccentricity. This result stands in contrast to the
363 result for P cells in which semisaturation, was inversely correlated with eccentricity ($r =$
364 -0.36 ; $p = 0.018$ vs. $r = 0.17$; $p = 0.273$) as previously observed (Solomon, White & Martin,
365 1999). Blue-off cells (green cross symbols, Fig. 4A,C,E) had similar characteristics to blue-on
366 cells but the number of cells is too small to make statistical comparisons. In comparison to a
367 simplified model in which the exponent term is held constant (see Methods section), the
368 expansive nonlinearity of Eq. 1 was necessary to explain the responses for a majority (29/44,
369 65%) of blue-on cells. Interestingly, the addition of an expansive term also improved the fits
370 for a substantial fraction (26/53, 49%) of P cells. On the other hand, the use of a
371 supersaturating Naka-Rushton curve (Eq. 3) did not significantly improve the fit to the data
372 for any cell, and non-monotonic responses were never observed in blue-on cells. Either an
373 expansive or a thresholding nonlinearity (Eq. 4) could adequately fit the data overall.
374 However, only the expansive nonlinearity model (Eq. 1) could consistently predict responses
375 at the contrast threshold. For blue-on cells, the overall RMS error of the expansive
376 nonlinearity model was not significantly different to the overall RMS error of the threshold
377 model (3.7 ± 1.4 imp/s vs. 3.9 ± 1.5 imp/s, respectively, $p = 0.34$, paired Wilcoxon test).

378 Response saturation is customarily associated with contrast gain control, which is
379 also manifest as advance in response phase with increasing contrast (Shapley & Victor,
380 1981; Kaplan & Benardete, 2001). On comparing response phase at half-maximum and
381 maximum contrast for preferred chromatic direction we found substantial phase advance in

382 MC cells (37.4 ± 18 degrees, $n = 22$), as would be expected (Yeh et al., 1995a; Levitt, Shumer,
383 Sherman & Spear, 2001; Solomon, Lee & Sun, 2006). Phase advance in MC cells was
384 significantly greater ($p < 0.02$, Kruskal-Wallis test) than the (negligible) phase advance in PC
385 cells (6.0 degrees ± 13 , $n = 46$) and blue-on cells (3.3 ± 9 , $n = 44$); there was no difference
386 between PC cells and blue-on cells ($p = 0.95$, Kruskal-Wallis test). There was no clear sign of
387 correlation between semisaturation constant and phase advance in blue-on cells ($r^2 < 0.01$,
388 $p = 0.82$). These data suggest that blue-on cells do not show contrast gain control to any
389 great extent. A more extensive analysis of response timing may be of interest for future
390 work.

391 *Achromatic responses arise from the summation of chromatic signals*

392 Blue-on cells integrate S cone signals with ML cone signals, and it is clear from Figure 4 that
393 there is variation between the S cone and ML cone responses within individual cells. We
394 showed above that this variation may be due to S and ML signals having different contrast
395 response characteristics at the level of the outer retina. If this is the case, then the
396 integrated responses to co-stimulation of S and ML cones is given by the sum of the
397 responses to cone stimuli, which could lead to non-monotonic achromatic contrast
398 responses (Fig. 1A, Eq. 5). Alternatively, the S cone and ML cone inputs to the blue-on cell
399 may be approximately linear, in which case the integrated output cannot be expressed
400 exactly as the sum of the component responses, but must be monotonic with increasing
401 contrast (Fig. 1B, Eq. 6).

402 Figure 5 shows a particularly illustrative example of a blue-on cell's responses where
403 the predictions made by these two models diverge. Figure 5A shows the cell's responses as
404 a function of contrast with fitted Naka-Rushton curves, as given by Eq. 6, for S and ML cone

405 stimuli. Chromatic contrast is expressed relative to stimulus cone contrast (80% for S and
406 ML cones). Figure 5B shows the measured achromatic contrast response function, along
407 with predicted contrast response functions given by fitting the two competing models to the
408 S and ML cone response data. The model with separable contrast mechanisms (dashed line,
409 Fig. 5B) predicts a non-monotonic achromatic contrast response. The non-monotonic
410 prediction arises because the expansive nonlinearity for ML-off is weaker than that for S-on,
411 predicting response cancellation at high but not intermediate contrast. The measured data,
412 however, falls on the curve predicted by the summation of linear cone inputs which are
413 distorted by a nonlinearity post-integration. Figure 5C shows the amplitude and phase of
414 the responses in the complex plane.

415 Overall, the weight of experimental evidence favors the model where summation of
416 linear cone inputs occurs prior to non-linear distortion, as described in Eq. 6 and illustrated
417 in Figure 1B. Across the population of blue-on cells, non-monotonic achromatic contrast
418 responses were never observed. Most cells could be reasonably fit by either model, as
419 would be expected if the cells are operating in the linear regime of their contrast response
420 functions. Figure 6 shows measured vs. predicted responses to achromatic (S + ML) and
421 mixed chromatic (S – ML) stimuli for the population of cells tested. Figure 6A shows the
422 predictions of Eq. 6 for achromatic (S + ML) stimulation (median RMS error 8.1 imp/s),
423 Figure 6B shows the predictions of Eq. 6 for mixed chromatic (S – ML) co-stimulation
424 (median RMS error 5.4 imp/s), Figure 6C shows the predictions of Eq. 5 for achromatic (S +
425 ML) stimulation (median RMS error 8.3 imp/s), and Figure 6D shows the predictions of Eq. 5
426 for S – ML stimulation (median RMS error 11.0 imp/s). The two models perform similarly in
427 prediction of achromatic responses ($p = 0.66$, 2-way KW), but the linear inputs model clearly

428 outperforms the separable contrasts model for chromatic (S – ML) stimulation ($p < 0.01$,
429 2-way KW).

430 *Amplitude and timing of opponent inputs to blue-on and blue-off cells*

431 Figure 7 shows, for the data collected using 5 Hz stimulation, the amplitude and phase of
432 responses to maximum-contrast S cone (Fig. 7A), ML cone (Fig. 7B), achromatic (Fig. 7C),
433 and S – ML stimulation (Fig. 7D) in the complex plane. Figures 7C and 7D also show (square
434 symbols) the distributions of achromatic and S – ML responses predicted by a vector sum of
435 S and ML inputs. There are four main points to take from these data. Firstly, as expected,
436 the S and ML responses cluster around close-to-opposite phase, consistent with S-on and
437 ML-off excitation. The mean phase delay between S and ML was 187 deg, equivalent to an
438 additional 3.6 ms at 5 Hz. Secondly, there is considerable variability in response phase
439 across the population for all stimuli. As the data of figure 7 were collected at varying spatial
440 frequencies, some variation in the observed response phases is due to offset of the centre
441 of the receptive field from the centre of the stimulus patch. The true response phases to
442 uniform stimulus are less variable than this figure implies – the circular standard deviation
443 of the response phases to spatially uniform 5 Hz S cone stimulation is 22.4° ($n = 40$),
444 equivalent to ± 12.4 ms at 5 Hz. Thirdly, for most (but not all) blue-on cells the phase of the
445 response to achromatic modulation is close to that for S cone modulation (circular $r = 0.42$,
446 $p < 0.02$). Finally, the fit predictions for achromatic and S – ML stimuli show heavy overlap in
447 phase space with the measured values, most evidently for S – ML stimuli (Fig. 7D). The
448 reader should note that these data are also consistent with the "sum-then-distort" contrast
449 integration model described above (Eq. 6, Fig 1B, Fig. 6).

450 Figure 7E shows on a per-cell basis the amplitude and phase of responses to

451 maximum-contrast S cone, ML cone, together with measured achromatic (S + ML) response
452 (black vector) and the vector sum prediction (magenta square symbols). Responses are
453 normalized to the maximum response amplitude, shown at bottom of each sub-plot. Here
454 we see that the broad distribution of response phase across the population belies some
455 hidden regularity, by revealing that the S and ML response phases are correlated on a cell by
456 cell basis (circular $r = 0.61$, $p < 0.01$). Responses to achromatic stimuli are attributable to
457 differences in amplitude and/or timing of the S and ML inputs. Two example cells are
458 marked in Figure 7E. The cell in the first example (open arrowhead, Fig. 7E [68, bottom left])
459 shows identical amplitude for S and ML inputs, but the ML input lags the S input by 209° ,
460 predicting a vigorous on-type achromatic response. For the second, [54, upper right] the
461 response phase difference is 187° but the S input amplitude is greater than the ML input
462 amplitude, again predicting a (weak) achromatic on-type response. These data show that
463 the gain and timing of S and ML inputs jointly determine responses to non-cone-isolating
464 stimuli.

465 *Spatial properties of S and ML inputs to blue-on cells*

466 A variety of receptive field structures was found for blue-on cells, as illustrated in Figure 8.
467 The simplest model (spatially coextensive S and ML subfields consistent with classical “type
468 II” organization), best fit the responses of 15 of 47 cells (32%). An example of the receptive
469 field structure of a type II cell is shown in Figure 8A. The associated S cone, ML cone, and
470 achromatic tuning curves and fitted Gaussians are shown in Figure 8B, and the S and ML
471 cone responses are plotted in the complex plane in Figure 8C. These cells rarely showed
472 achromatic responses at any spatial frequency; however, spatially low-pass achromatic
473 responses were observed in 5 of the 15 type II cells. In 5 cells (11%), a S-on subfield and a

474 ML-off subfield of different sizes (which were not necessarily concentric) were sufficient to
475 explain the cell's response, consistent with the receptive field organization described in
476 Tailby et al. (2010). An example of this receptive field structure is shown in Figure 8D, along
477 with the associated fitted S cone, ML cone, and achromatic tuning curves (Fig. 8E) and
478 location in the complex plane (Fig. 8F). Note the band-pass response to achromatic
479 stimulation. In 13 cells (28%), the S cone input had spatial bandpass tuning without
480 evidence of a corresponding bandpass characteristic for ML cone input. Responses of such
481 cells are consistent with the presence of an S cone surround. An example of such a cell is
482 shown in Figure 8G, along with the associated fitted S cone, ML cone, and achromatic tuning
483 curves (Fig. 8H) and location in the complex plane (Fig. 8I). Both the achromatic and the S
484 cone spatial frequency tuning curves show response roll-off at low spatial frequencies.
485 Bandpass achromatic responses were present in 6 of 13 cells, with low-pass responses
486 observed in a further 2 cells. The remainder (14 out of 47 cells, 30%) required both an S-off
487 surround and a weak ML-on surround to explain the cell's response. An example of such a
488 receptive field is shown in Figure 8J, along with the associated fitted S cone, ML cone, and
489 achromatic tuning curves (fig. 8K) and location in the complex plane (fig. 8L). As we show
490 below, overall the ML surrounds were weaker than S surrounds, and made only a small but
491 significant improvement in fit quality. Spatial bandpass achromatic responses were more
492 frequent in this population, being present in 9 out of 14 cells.

493 Figure 9 shows radius and volume of S cone and ML cone subunits for blue-on and
494 blue-off cells, and compares these parameters with ML cone inputs to P cells. Summary
495 statistics for the data shown in Figure 9 (A, B, C, E) are given in Table 3. For blue-on cells, the
496 S-on subfield has a marginally smaller radius than the ML-off subfield (Fig. 9A, $p = 0.10$,

497 paired Wilcoxon test), but has, on average, significantly larger volume (Fig. 9B, $p < 0.01$,
 498 paired Wilcoxon). The S-on subfield radii increased with foveal eccentricity (Kendall's tau =
 499 0.31, $p < 0.01$) as has been reported previously (Tailby et al., 2008b). Surprisingly, the
 500 eccentricity-dependence was less pronounced for the ML-off subfields (tau = 0.15, $p =$
 501 0.17). The reason for this difference is not clear. The reported receptive field radii for the
 502 S-on and ML-on subunits are within the range which would be expected based on the
 503 dendritic arbor of the SBS RGC: $0.50^\circ \pm 0.22^\circ$ for S cones and $0.26^\circ \pm 0.15^\circ$ for ML cones (see
 504 also Tailby et al., 2010).

505

Table 3

Blue-on cells	Radius (deg)	Volume (imp/s % ⁻¹)	Frequency
S-cone on-polarity centre	$0.38^\circ \pm 0.37^\circ$	1.58 ± 1.15	100% (47/47)
ML-cone off-polarity centre	$0.40^\circ \pm 0.33^\circ$	1.29 ± 0.98	100% (47/47)
S-cone off-polarity surround	$1.08^\circ \pm 0.69^\circ$	1.09 ± 1.13	55% (26/47)
ML-cone on-polarity surround	$2.41^\circ \pm 5.44^\circ$	1.33 ± 1.56	30% (14/47)
P cell centre (ML-cone)	$0.10^\circ \pm 0.10^\circ$	1.19 ± 0.48	100% (72/72)
P cell surround (ML-cone)	$0.80^\circ \pm 0.88^\circ$	0.91 ± 0.40	85% (61/72)

506 All values mean \pm SD

507 Figure 9C compares ML centre and surround radius for P cells against the S-on, S-off,
 508 ML-off, and ML-on subunits (where detectable) of blue-on cells. Figure 9D shows the ratios
 509 of these quantities. As expected (for review, see Martin & Lee, 2014), P cell centre radii are
 510 significantly smaller than S-on and ML-off radii in blue-on cells ($p < 0.01$ for both
 511 comparisons, independent Wilcoxon). Also as expected, the S-on/ML-off ratio for blue-on
 512 cell RF radii (0.993 ± 0.408) is greater than the ratio of P cell centre/surround radii ($0.203 \pm$
 513 0.173 , $p < 0.01$, n-way KW), reflecting their distinct origins in retinal wiring (Field et al.,
 514 2007; Crook et al., 2009). Where measurable, the blue-on cell S-on/S-off and ML-off/ML-on
 515 radius ratios (0.347 ± 0.218 and 0.365 ± 0.186 , respectively) were also distinguishable from

516 P cells ($p < 0.01$ and $p = 0.04$, respectively); perhaps unsurprisingly, the distribution of
517 ML-cone centre/surround ratios was more similar to the distribution of P cell
518 centre/surround ratios.

519 Figure 9E compares ML centre and surround volumes for P cells against the S-on,
520 S-off, ML-on and ML-off subunits (where detectable) for blue-on cells. Figure 9F shows the
521 ratios of these quantities. In contrast to the marked differences in radii, P cell centre
522 volumes were not significantly different from S or ML subunit volumes in blue-on cells ($p =$
523 0.09 and $p = 0.28$ for S cone and ML cone subfields, respectively, independent Wilcoxon).
524 Correspondingly, the S-on/ML-off volume ratio in blue-on cells (1.470 ± 1.037) was close to
525 the centre/surround volume ratio in P cells (1.596 ± 0.860 , $p = 0.414$, independent Wilcoxon).
526 This result may help explain why P cells and blue-on cells both respond weakly to
527 achromatic contrast at low spatial frequencies: the antagonistic subunit sizes are very
528 different in P cells and blue-on cells, yet the integrated sensitivities are similar and
529 well-matched. On the other hand, where detectable, the volume ratios S-on/S-off and
530 ML-off/ML-on in blue-on cells were higher (2.613 ± 1.952 and 2.286 ± 1.070 , respectively).
531 In other words, the spatially antagonistic subunits in blue-on cells contribute only weakly to
532 shaping the cells' overall response.

533 **Discussion**

534 We show that when stimulated with low-to-moderate S cone or ML cone contrast, blue-on
535 cells show predominantly linear contrast response functions. Mild response saturation at
536 high contrast and some expansive nonlinearity at low contrasts are evident.

537 The degree of response saturation in blue-on cells shows heavy overlap with that of

538 PC cells and is much weaker than that of MC cells (Fig 4A, B). The expansive nonlinearity
539 could potentially sharpen blue-on cells' chromatic selectivity as proposed for cortical
540 neurons (Heeger, 1992; DeValois, Cottaris, Elfar, Mahon & Wilson, 2000; Solomon, Peirce &
541 Lennie, 2004; Solomon & Lennie, 2005), but our stimulus set was too restricted to address
542 this possibility. The fact that blue-on ganglion cells show little sign of expansive nonlinearity
543 (Yeh et al., 1995a; Crook et al., 2009) suggests that this distortion occurs either at the
544 ganglion cell to LGN cell synapse or at the LGN spike output stage. Expansive nonlinearity at
545 low contrasts is also a feature of PC cell responses in LGN of awake and anesthetized
546 macaque monkeys (Alitto, Moore, Rathbun & Usrey, 2011), thus its presence in the PC cells
547 and blue-on cells we recorded is not simply attributable to a species difference, or
548 sufentanil anesthesia, or a switch of the LGN into a non-responsive "burst" mode (Sherman,
549 1996). It is important to note however that the effects we see in LGN are much milder than
550 the nonlinearities in cortical cell responses reported in the studies cited above and
551 elsewhere.

552 We found that responses to simultaneous recruitment of both S cones and ML cones
553 are consistent with integration of linear S cone and ML cone signals prior to non-linear
554 distortion of the integrated signal. This result is consistent with measurements of linear S
555 cone and ML cone synaptic inputs to SBS ganglion cells (Chichilnisky & Baylor, 1999; Field et
556 al., 2007; Crook et al., 2009). In common with these previous reports, in our experimental
557 setup we could only access a limited range of intensities (maximum 120 cd m^{-2}), where the
558 cone signals are likely operating in a linear range. Lee, Valberg and colleagues (1983, 1987)
559 used narrow band spectral lights to show saturating cone inputs are needed to account for
560 responses of blue-on cells at high intensities ($> 500 \text{ cd m}^{-2}$). The presence of response

561 saturation at a pre-cortical level may also help to explain some features of cortical contrast
562 response (Solomon & Lennie, 2005) and fits within some models of the LGN's computational
563 contribution to vision (Dan, Atick & Reid, 1996; Mante, Frazor, Bonin, Geisler & Carandini,
564 2005).

565 Our observation of blue-on LGN cells with varying receptive field structures may also
566 have implications for current theories on the retinal circuitry underpinning blue-on cells.
567 One current theory is that the SBS ganglion cell receives convergent input from a S
568 cone-specific bipolar cell (BB) as well as one or more classes of diffuse off-type bipolar cell
569 (DB) (Crook et al., 2009; Dacey, Crook & Packer, 2013). The S cone signal from the BB input
570 is expected to carry an off-polarity ML cone surround (Packer, Verweij, Li, Schnapf & Dacey,
571 2010) and the ML cone signal from the DB cells carries an on-polarity ML cone surround
572 (Dacey, Diller, Verweij & Williams, 2000). Crook et al. (2009) proposed that mutual
573 anihilation of these ML surround signals generate spatially co-extensive S cone and ML
574 cone receptive fields (Crook et al., 2009, Dacey et al., 2014). Cell-specific imbalances in this
575 mechanism could be expected to produce a distribution of ML cone surrounds, which could
576 partially explain the variation in receptive field structure observed in blue-on cells in the
577 LGN. The convergent BB+DB input theory, however, fails to provide an explanation for the
578 off-polarity S cone surround that we observed in 57% of cells, nor why we did not observe
579 blue-on cells with ML cone, but not S cone, surrounds. It is possible that the S cone surround
580 is mediated by inhibitory amacrine cell input onto SBS ganglion cells (Ghosh & Grünert,
581 1999); however, if this were indeed the case, why have inhibitory S cone surround
582 responses not been reported in SBS ganglion cells? An alternative possibility is that the S
583 cone off-polarity surround is a consequence of lateral inhibition in the LGN.

584 In summary, the image of blue-on and blue-off cells which emerges from these data is
585 largely compatible with the blue-yellow color opponent channel originally hypothesized by
586 Hering (Hering, 1878; Jameson & Hurvich, 1955). The (lilac-lime) axis of maximum sensitivity
587 for blue-on cells is not exactly aligned with the perceptual blue-yellow axis proposed by
588 Hering. But other properties of blue-on cells conform nicely to requirement of a chromatic
589 opponent channel. Blue-on cells give responses of opposite polarity to short-wave and
590 medium-wave regions of the spectrum. These responses show mutual antagonism, yielding
591 weak responses to achromatic (S + ML) stimuli and strong responses to mixed chromatic
592 (S–ML) stimuli. Further, the spatial properties of the antagonistic S-on and ML-off subunits
593 are well-matched, yielding vigorous low-pass responses to chromatic contrast. Spatial
594 centre-surround structure in blue-on receptive fields, where detectable, was weak and
595 variable. One interpretation of this variability is that central mechanisms may not prioritize
596 spatial contrast enhancement through blue-on cells. In this case the question whether
597 blue-on cells are strictly Type II or not becomes largely academic. As a population these cells
598 are clearly specified to favour chromatic over spatial contrast.

599

600 **Acknowledgements**

601 We thank A. Camp, S. Chen, K. Cheong, S. S. Solomon (no relation to S. G. Solomon) and C.

602 Tailby for assistance with data collection, and C. Guy and A. Demir for technical assistance.

603 Supported by Australian National Health and Medical Research Council Grants 1027913 and

604 1005427 and Australian Research Council grant CE140100007.

605

606 **References**

- 607 Alitto, H.J., Moore, B.D., Rathbun, D.L. & Usrey, W.M. (2011). A comparison of visual responses in
608 the lateral geniculate nucleus of alert and anaesthetized macaque monkeys. *Journal of*
609 *Physiology*, 589: 87-99.
- 610 Benardete, E.A. & Kaplan, E. (1999). The dynamics of primate M retinal ganglion cells. *Visual*
611 *Neuroscience*, 16: 355-368.
- 612 Blessing, E.M., Solomon, S.G., Hashemi-Nezhad, M., Morris, B.J. & Martin, P.R. (2004). Chromatic and
613 spatial properties of parvocellular cells in the lateral geniculate nucleus of the marmoset
614 (*Callithrix jacchus*). *Journal of Physiology*, 557: 229-245.
- 615 Brainard, D.H. (1996) Cone contrast and opponent modulation color spaces. In: Kaiser, P.K. &
616 Boynton, G.M. (Eds.), *Human Color Vision* (pp.563-577), Washington, D. C.: Optical Society of
617 America.
- 618 Buzás, P., Kóbor, P., Petykó, Z., Telkes, I., Martin, P.R. & Lénárd, L. (2013). Receptive field properties
619 of color opponent neurons in the cat lateral geniculate nucleus. *Journal of Neuroscience*, 33:
620 1451-1461.
- 621 Cheong, S.K. & Pietersen, A.N. (2014). Antidromic latency of magnocellular, parvocellular, and
622 koniocellular (Blue-ON) geniculocortical relay cells in marmosets. *Visual Neuroscience*, 31:
623 263-273.
- 624 Cheong, S.K., Tailby, C., Solomon, S.G. & Martin, P.R. (2013). Cortical-like receptive fields in the
625 lateral geniculate nucleus of marmoset monkeys. *Journal of Neuroscience*, 33: 6864-6876.
- 626 Chichilnisky, E.J. & Baylor, D.A. (1999). Receptive-field microstructure of blue-yellow ganglion cells in
627 primate retina. *Nature Neuroscience*, 2: 889-893.

628 Crook, J.D., Davenport, C.M., Peterson, B.B., Packer, O.S., Detwiler, P.B. & Dacey, D.M. (2009).
629 Parallel ON and OFF cone bipolar inputs establish spatially coextensive receptive field
630 structure of blue-yellow ganglion cells in primate retina. *Journal of Neuroscience*, 29:
631 8372-8387.

632 Dacey, D.M. (2004) Origins of perception: Retinal ganglion cell diversity and the creation of parallel
633 visual pathways. In: Gazzaniga, M.S. (Ed.), *The Cognitive Neurosciences III* (pp.281-301),

634 Dacey, D.M., Crook, J.D. & Packer, O.S. (2013). Distinct synaptic mechanisms create parallel S-ON
635 and S-OFF color opponent pathways in the primate retina. *Visual Neuroscience*, 1-13.

636 Dacey, D.M., Diller, L.C., Verweij, J. & Williams, D.R. (2000). Physiology of L- and M-cone inputs to H1
637 horizontal cells in the primate retina. *Journal of the Optical Society of America A, Optics and*
638 *Image Science*, 17: 589-596.

639 Dacey, D.M. & Lee, B.B. (1994). The 'blue-on' opponent pathway in primate retina originates from a
640 distinct bistratified ganglion cell type. *Nature*, 367: 731-735.

641 Dan, Y., Atick, J.J. & Reid, R.C. (1996). Efficient coding of natural scenes in the lateral geniculate
642 nucleus: experimental test of a computational theory. *Journal of Neuroscience*, 16:
643 3351-3362.

644 DeValois, R.L., Cottaris, N.P., Elfar, S.D., Mahon, L.E. & Wilson, J.A. (2000). Some transformations of
645 color information from lateral geniculate nucleus to striate cortex. *Proceedings of the National*
646 *Academy of Sciences of the USA*, 97: 4997-5002.

647 Enroth-Cugell, C. & Robson, J. (1966). The contrast sensitivity of retinal ganglion cells of the cat.
648 *Journal of Physiology*, 187: 517-552.

649 Enroth-Cugell, C., Robson, J.G., Schweitzer-Tong, D.E. & Watson, A.B. (1983). Spatio-temporal
650 interactions in cat retinal ganglion cells showing linear spatial summation. *Journal of*
651 *Physiology*, 341: 279-307.

652 Field, G.D., Sher, A., Gauthier, J.L., Greschner, M., Shlens, J., Litke, A.M. & Chichilnisky, E.J. (2007).
653 Spatial properties and functional organization of small bistratified ganglion cells in primate
654 retina. *Journal of Neuroscience*, 27: 13261-13272.

655 Frishman, L.J., Freeman, A.W., Troy, J.B., Schweitzer-Tong, D.E. & Enroth-Cugell, C. (1987).
656 Spatiotemporal frequency responses of cat retinal ganglion cells. *Journal of General*
657 *Physiology*, 89: 599-628.

658 Ghosh, K.K. & Grünert, U. (1999). Synaptic input to small bistratified (blue-On) ganglion cells in the
659 retina of a New World monkey, the marmoset *Callithrix jacchus*. *Journal of Comparative*
660 *Neurology*, 413: 417-428.

661 Heeger, D.J. (1992). Normalization of cell responses in cat striate cortex. *Visual Neuroscience*, 9:
662 181-197.

663 Hering, E. (1878) *Grundzüge einer Theorie des Farbensinnes* (originally published in 1874). (Ed.), Zur
664 *Lehre vom Lichtsinn* (pp.107-141), Wien: Gerald u. Söhne.

665 Jameson, D. & Hurvich, L.M. (1955). Some quantitative aspects of an opponent-colors theory:I.
666 Chromatic responses and spectral saturation. *Journal of the Optical Society of America*, 45:
667 546-552.

668 Kaplan, E. & Benardete, E. (2001). The dynamics of primate retinal ganglion cells. *Progress in Brain*
669 *Research*, 134: 17-34.

670 Kaplan, E. & Shapley, R.M. (1986). The primate retina contains two types of ganglion cells, with high
671 and low contrast sensitivity. *Proceedings of the National Academy of Sciences of the USA*, 83:
672 2755-2757.

673 Lee, B.B., Valberg, A., Tigwell, D.A. & Tryti, J. (1987). An account of responses of spectrally opponent
674 neurons in macaque lateral geniculate nucleus to successive contrast. *Proceedings of the*
675 *Royal Society (London) B*, 230: 293-314.

676 Lee, B.B., Virsu, V. & Elepfandt, A. (1983). Cell responses in dorsal layers of macaque lateral
677 geniculate nucleus as a function of intensity and wavelength. *Journal of Neurophysiology*, 50:
678 849-863.

679 Levitt, J.B., Shumer, R.A., Sherman, S.M. & Spear, P.D. (2001). Visual response properties of neurons
680 in the LGN of normally reared and visually deprived macaque monkeys. *Journal of*
681 *Neurophysiology*, 85: 2111-2119.

682 Mante, V., Frazor, R.A., Bonin, V., Geisler, W.S. & Carandini, M. (2005). Independence of luminance
683 and contrast in natural scenes and in the early visual system. *Nature Neuroscience*,

684 Martin, P.R. & Lee, B.B. (2014). Distribution and specificity of S-cone ("blue cone") signals in
685 subcortical visual pathways. (Review). *Visual Neuroscience*, 31: 177-187.

686 Martin, P.R., White, A.J.R., Goodchild, A.K., Wilder, H.D. & Sefton, A.E. (1997). Evidence that blue-on
687 cells are part of the third geniculocortical pathway in primates. *European Journal of*
688 *Neuroscience*, 9: 1536-1541.

689 Naka, K.-I. & Rushton, W.H. (1966). S-potentials from colour units in the retina of fish (*Cyprinidae*).
690 *Journal of Physiology*, 185: 536-555.

691 Packer, O.S., Verweij, J., Li, P.H., Schnapf, J.L. & Dacey, D.M. (2010). Blue-yellow opponency in
692 primate S cone photoreceptors. *Journal of Neuroscience*, 30: 568-572.

693 Peirce, J.W. (2007). The potential importance of saturating and supersaturating contrast response
694 functions in visual cortex. *Journal of Vision*, 7: 13.

695 Pietersen, A.N., Cheong, S.K., Solomon, S.G., Tailby, C. & Martin, P.R. (2014). Temporal response
696 properties of koniocellular (blue-on and blue-off) cells in marmoset lateral geniculate nucleus.
697 *Journal of Neurophysiology*, 112: 1421-1438.

698 Rodieck, R.W. & Stone, J. (1965). Analysis of receptive fields of cat retinal ganglion cells. *Journal of*
699 *Neurophysiology*, 28: 833-849.

700 Roy, S., Martin, P.R., Dreher, B., Saalmann, Y.B., Hu, D. & Vidyasagar, T.R. (2009). Segregation of
701 short-wavelength sensitive (S) cone signals in the macaque dorsal lateral geniculate nucleus.
702 *European Journal of Neuroscience*, 30: 1517-1526.

703 Schnapf, J.L., Nunn, B.J., Meister, M. & Baylor, D.A. (1990). Visual transduction in cones of the
704 monkey (*Macaca fascicularis*). *Journal of Physiology*, 427: 681-713.

705 Sclar, G., Maunsell, J.H.R. & Lennie, P. (1990). Coding of image contrast in central visual pathways of
706 the macaque monkey. *Vision Research*, 30: 1-10.

707 Shapley, R.M. & Victor, J.D. (1978). The effect of contrast on the transfer properties of cat retinal
708 ganglion cells. *Journal of Physiology*, 285: 275-298.

709 Shapley, R.M. & Victor, J.D. (1981). How the contrast gain control modifies the frequency responses
710 of cat retinal ganglion cells. *Journal of Physiology*, 318: 161-179.

711 Sherman, S.M. (1996). Dual response modes in lateral geniculate neurons: mechanisms and
712 functions. *Visual Neuroscience*, 13: 205-213.

713 Silveira, L.C.L., Lee, B.B., Yamada, E.S., Kremers, J., Hunt, D.M., Martin, P.R. & Gomes, F. (1999).
714 Ganglion cells of a short wavelength sensitive cone pathway in New World monkeys:
715 Morphology and Physiology. *Visual Neuroscience*, 16: 333-343.

716 Solomon, S.G., Lee, B.B. & Sun, H. (2006). Suppressive surrounds and contrast gain in
717 magnocellular-pathway retinal ganglion cells of macaque. *Journal of Neuroscience*, 26:
718 8715-8726.

719 Solomon, S.G., Lee, B.B., White, A.J., Rüttiger, L. & Martin, P.R. (2005). Chromatic organization of
720 ganglion cell receptive fields in the peripheral retina. *Journal of Neuroscience*, 25: 4527-4539.

721 Solomon, S.G. & Lennie, P. (2005). Chromatic gain controls in visual cortical neurons. *Journal of*
722 *Neuroscience*, 25: 4779-4792.

723 Solomon, S.G., Peirce, J.W. & Lennie, P. (2004). The impact of suppressive surrounds on chromatic
724 properties of cortical neurons. *Journal of Neuroscience*, 24: 148-160.

725 Solomon, S.G., White, A.J.R. & Martin, P.R. (1999). Temporal contrast sensitivity in the lateral
726 geniculate nucleus of a New World monkey, the marmoset *Callithrix jacchus*. *Journal of*
727 *Physiology*, 517: 907-917.

728 Szmajda, B.A., Martin, P.R. & Grünert, U. (2008). Retinal ganglion cell inputs to the koniocellular
729 pathway. *Journal of Comparative Neurology*, 510: 251-268.

730 Tailby, C., Dobbie, W.J., Hashemi-Nezhad, M., Forte, J.D. & Martin, P.R. (2010). Receptive field
731 asymmetries produce color-dependent direction selectivity in primate lateral geniculate
732 nucleus. *Journal of Vision*, 10: 1-18.

733 Tailby, C., Solomon, S.G. & Lennie, P. (2008a). Functional asymmetries in visual pathways carrying
734 S-cone signals in macaque. *Journal of Neuroscience*, 28: 4078-4087.

735 Tailby, C., Szmajda, B.A., Buzás, P., Lee, B.B. & Martin, P.R. (2008b). Transmission of blue (S) cone
736 signals through the primate lateral geniculate nucleus. *Journal of Physiology*, 586: 5947-5967.

737 White, A.J.R., Goodchild, A.K., Wilder, H.D., Sefton, A.E. & Martin, P.R. (1998). Segregation of
738 receptive field properties in the lateral geniculate nucleus of a New-World monkey, the
739 marmoset *Callithrix jacchus*. *Journal of Neurophysiology*, 80: 2063-2076.

740 Wiesel, T.N. & Hubel, D. (1966). Spatial and chromatic interactions in the lateral geniculate body of
741 the rhesus monkey. *Journal of Neurophysiology*, 29: 1115-1156.

742 Yeh, T., Lee, B.B. & Kremers, J. (1995a). Temporal response of ganglion cells of the macaque retina to
743 cone-specific modulation. *Journal of the Optical Society of America A*, 12: 456-464.

744 Yeh, T., Lee, B.B., Kremers, J., Cowing, J.A., Hunt, D.M., Martin, P.R. & Troy, J.B. (1995b). Visual
745 responses in the lateral geniculate nucleus of dichromatic and trichromatic marmosets
746 (*Callithrix jacchus*). *Journal of Neuroscience*, 15: 7892-7904.

747

748 **Figure Legends**

749 **Figure 1**

750 Prospective models for cone opponency. A: nonlinear inputs, linearly separable output
751 model corresponding to Eq. 5 B: linear input, nonlinear output model corresponding to Eq. 6

752 **Figure 2**

753 Cell Type classification. Example response raster plots and PSTHs showing responses to brief
754 (0.2s) increments and decrements of ML- and S cone contrast. Representative blue-on
755 koniocellular (A), parvocellular (B), and magnocellular (C) cells are shown. D: Response of
756 cell (A) to S- and ML cone-isolating drifting gratings (1 cyc/deg, 5 cyc/s, 4° aperture) as a
757 function of cone contrast. Error bars, in some cases smaller than the data point, are \pm std.
758 error. Arrowhead shows the contrast used for the data shown in (E). E: Response of cell (A)
759 to S- and ML cone-isolating drifting gratings (50% contrast, 5 cyc/s) as a function of grating
760 spatial frequency. F, G: Responses of cell (B) to achromatic flashing dot and drifting gratings
761 (7.1 cyc/s, 2° aperture (F) and 8° aperture (G)). H, I: Response of cell (C) to achromatic
762 flashing dot and drifting gratings (5 cyc/s, 1° aperture).

763

764 **Figure 3**

765 Typical contrast responses for a blue-on and blue-off cell. A: Raster plots for 2 s
766 presentations of 5 Hz S cone-isolating, ML cone-isolating, achromatic S+ML, and mixed S-ML
767 2° flashing dot, organized by stimulus contrast, for a typical blue-on cell. B: Mean firing rate
768 and first 5 Fourier components of the response at maximum contrast. The zeroth and first
769 harmonic contain the majority of the response power. C: First-harmonic contrast response
770 curves for the data presented in (A), showing response amplitude. Error bars, typically

771 smaller than the data point, are \pm std. error. Smooth curves show fits of Eq. 1 to the data. D:
772 Complex plane plot for the data presented in (A), showing the amplitude and phase of the
773 first-harmonic response. This cell has an on-phase response to S cone stimulation and an
774 off-phase response to ML cone stimulation. E, F, G, H: Responses of a blue-off cell to a 4Hz
775 drifting grating (0.1 cyc/deg, 8° aperture) of the above chromaticities. This cell has an
776 off-phase response to S cone stimulation and an on-phase response to ML cone stimulation.

777

778 **Figure 4**

779 Scatterplots and distributions of fitted Naka-Rushton equation parameters. A: Scatterplot of
780 fitted semi-saturation constants for S- and ML cone-isolating stimuli for blue-on and blue-off
781 cells. Lines of unity shown in grey. Values over 100% indicate non-saturating responses. B:
782 Distributions of fitted semi-saturation constants for ML cone-isolating stimuli for blue-on, P,
783 and M cells. Hatching indicates truncation of plotted distributions. C: Scatterplot of contrast
784 gains for S- and ML cone-isolating stimuli for blue-on and blue-off cells. D: Distributions of
785 contrast gains for ML cone-isolating stimuli for blue-on, P, and M cells. E: Scatterplot of
786 fitted exponents for S- and ML cone-isolating stimuli for blue-on and blue-off cells. F:
787 Distributions of fitted exponents for ML cone-isolating stimuli for blue-on, P, and M cells.

788 **Figure 5**

789 Illustrative example of difference in predictions made by Eq. 5 and Eq. 6 for a selected
790 sample cell. A: First-harmonic S- and ML cone contrast response functions. Error bars, in
791 most cases smaller than the data point, are \pm std. error. Smooth curves show fits of Eq. 6 to
792 the data. Open circles are S cone responses; filled circles are ML cone responses; black
793 diamonds are achromatic responses. B: Measured and predicted first-harmonic response to
794 achromatic stimulation. Dashed curve plots the achromatic response predicted by Eq. 5,

795 solid curve plots the achromatic response predicted by Eq. 6. C: Complex plane plot for the
796 data presented in (A) and (B), showing the amplitude and phase of the first-harmonic
797 response.

798 **Figure 6**

799 Predicted vs. measured response amplitudes for achromatic S+ML and mixed S – ML
800 stimulation. A,B: Scatterplot of predicted vs. measured achromatic (A) and “optimal” S – ML
801 (B) response amplitudes across all contrasts, excluding contrasts at which either S cone or
802 ML cone stimulation did not evoke a response > 5 imp/s. The model assuming linear inputs,
803 corresponding to fig. 1B, is used to generate predictions for each cell. C,D: Scatterplot of
804 predicted vs. measured achromatic (C) and “optimal” S – ML (D) response amplitudes across
805 contrasts. The model assuming separable nonlinear inputs, corresponding to fig. 1A, is used
806 to generate predictions for each cell.

807 **Figure 7**

808 Predicted vs. measured complex achromatic response across all blue-on cells measured at 5
809 Hz. A-D: Population summary of aggregate F1 response in the complex plane, for S cone-
810 isolating (B), ML cone-isolating (C), achromatic S + ML (D), and counter-phase chromatic S –
811 ML (E) stimuli. Open squares show predictions by Eq. 6 for (D) and (E). E: aggregate S
812 cone-isolating, ML cone-isolating, achromatic, and predicted achromatic responses for each
813 cell, arranged from most foveal (top left) to most peripheral (bottom right) and normalized
814 to each cell’s response (in imp/s), given in bottom right of each plot. Clockwise motion on
815 each dial indicates increasing phase lag. Off-phase responses fall in the shaded region of
816 each dial. Markers are as used in (B-E). Open arrowhead (lower left) indicates a cell in which
817 phase lag dominates the predicted achromatic response. Closed arrowhead (upper right)
818 indicates a cell in which response gain dominates the predicted achromatic response.

819 **Figure 8**

820 Examples of observed receptive field organization for blue-on cells, corresponding to the
821 model types listed in table 1. A: Example classical “type II” spatially coextensive receptive
822 field for a blue-on cell at 2.8° eccentricity. B: S- and ML cone contrast response functions
823 and measured achromatic contrast responses for the cell receptive field shown in (A). Error
824 bars, in some cases smaller than the data point, are \pm std. error. Smooth curves show fits of
825 Eq. 7 to the data. Open circles are S cone responses; filled circles are ML cone responses.
826 Dashed curve shows the predicted achromatic response. C: Complex plane plot for the data
827 presented in (A) and (B), showing the amplitude and phase of the first-harmonic response.
828 Smooth curve shows the amplitude and phase of the fitted model. D-F: Example simple
829 opponent blue-on cell at 0.7° eccentricity. Filled red circle shows the spatial extent of the
830 ML cone receptive field; open blue circle shows the spatial extent of the S cone receptive
831 field. G-I: Example cell with centre-surround organization of S cone inputs at 4.8°
832 eccentricity. Dashed blue circle shows the spatial extent of the S cone surround. J-L:
833 Example cell with centre-surround organization of both S cone inputs and ML cone inputs at
834 3.9° eccentricity. Filled dashed circle shows the spatial extent of the ML cone surround.
835

836 **Figure 9**

837 Scatterplots and distributions of fitted difference-of-Gaussians equation parameters.

838 A: Scatterplot of fitted receptive field radius for S- and ML cone inputs to blue-on and

839 blue-off cells. Cells with classical “type II” coextensive receptive fields fall on the line of

840 unity, shown in grey. B: Scatterplot of fitted receptive field volumes for S- and ML cone

841 inputs for blue-on and blue-off cells. C: Scatterplot of centre and surround radius for S cone

842 input to blue-on cells, ML cone input to blue-on cells, P on cells, and P off cells. Marker

843 legend per (F). D: Distributions of radius ratios. From left to right: ratio of S subfield to ML

844 subfield radius for blue-on cells; ratio of ML centre radius to ML surround radius for P on

845 cells, ratio of ML centre radius to ML surround radius for P off cells; ratio of S cone centre

846 radius to S cone surround radius for blue-on cells; ratio of ML centre radius to ML surround

847 radius for blue-on cells off cells. E: Scatterplot of centre and surround volume for S cone

848 input to blue-on cells, ML cone input to blue-on cells, P on cells, and P off cells.

849 F: Distributions of volume ratios, in the same format as panel D.

850

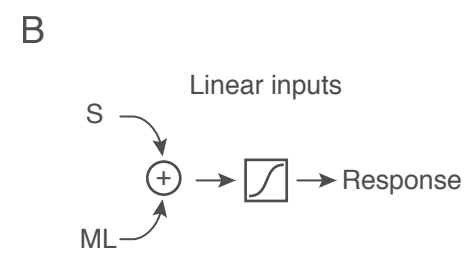
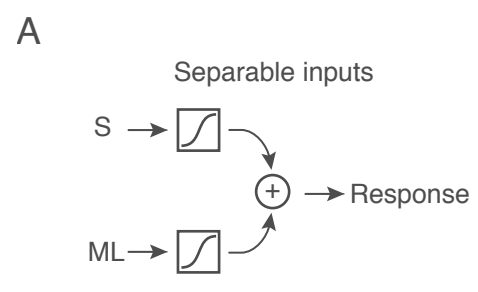


Figure 2

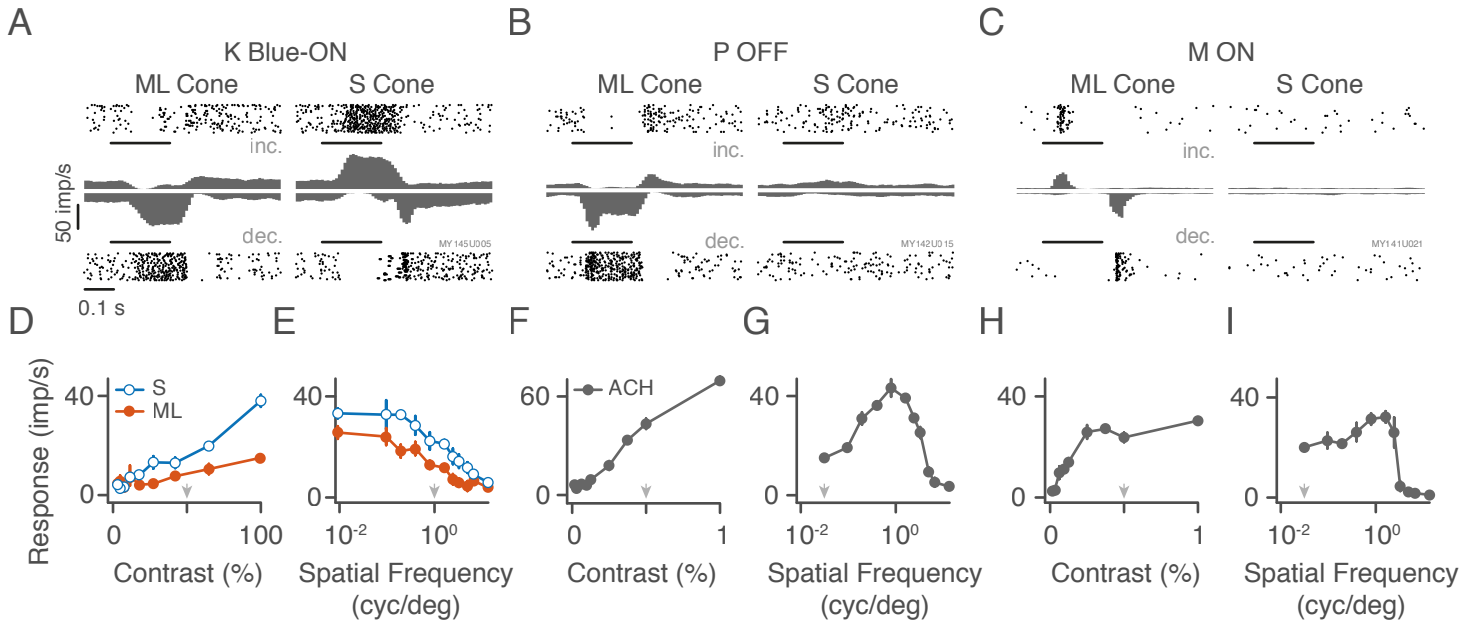


Figure 3

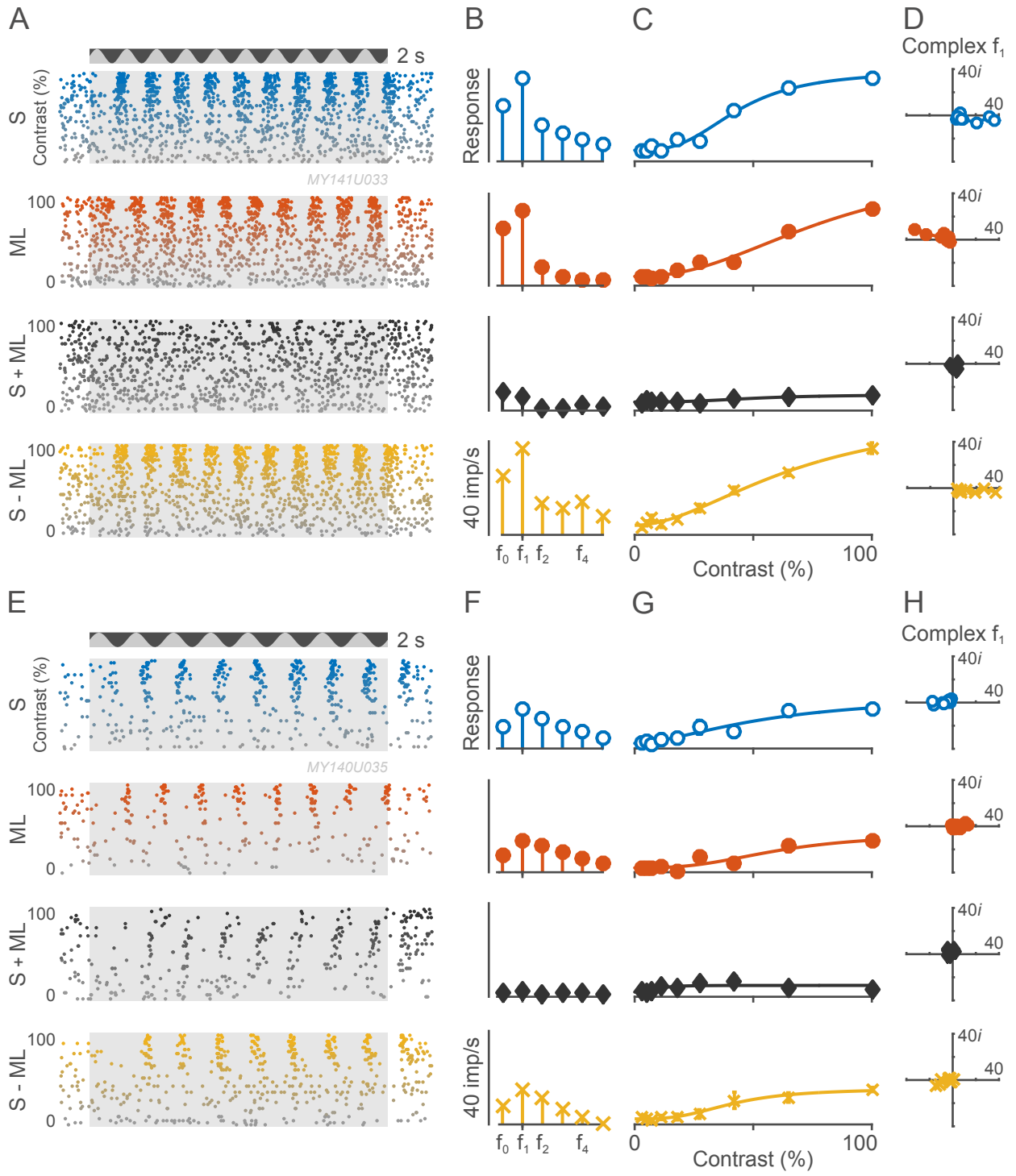


Figure 4

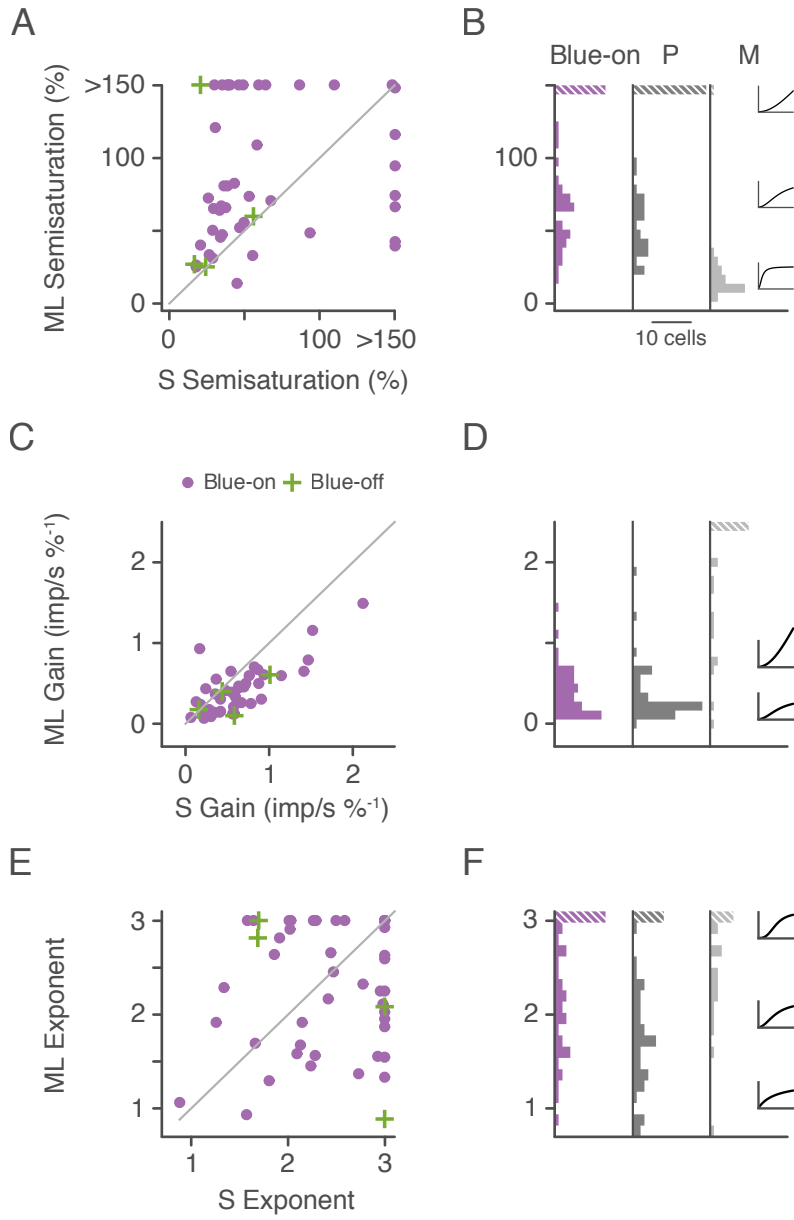


Figure 5

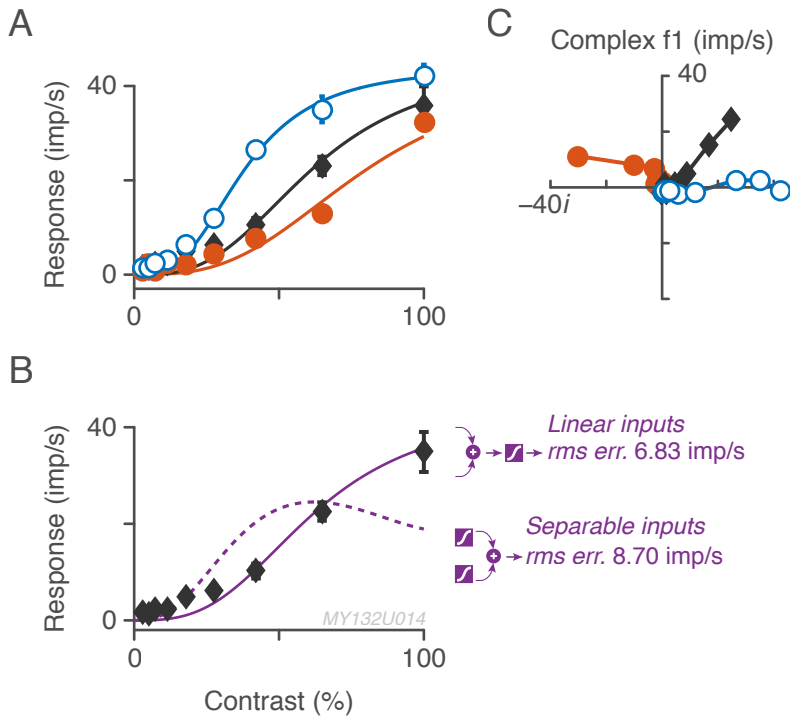


Figure 6

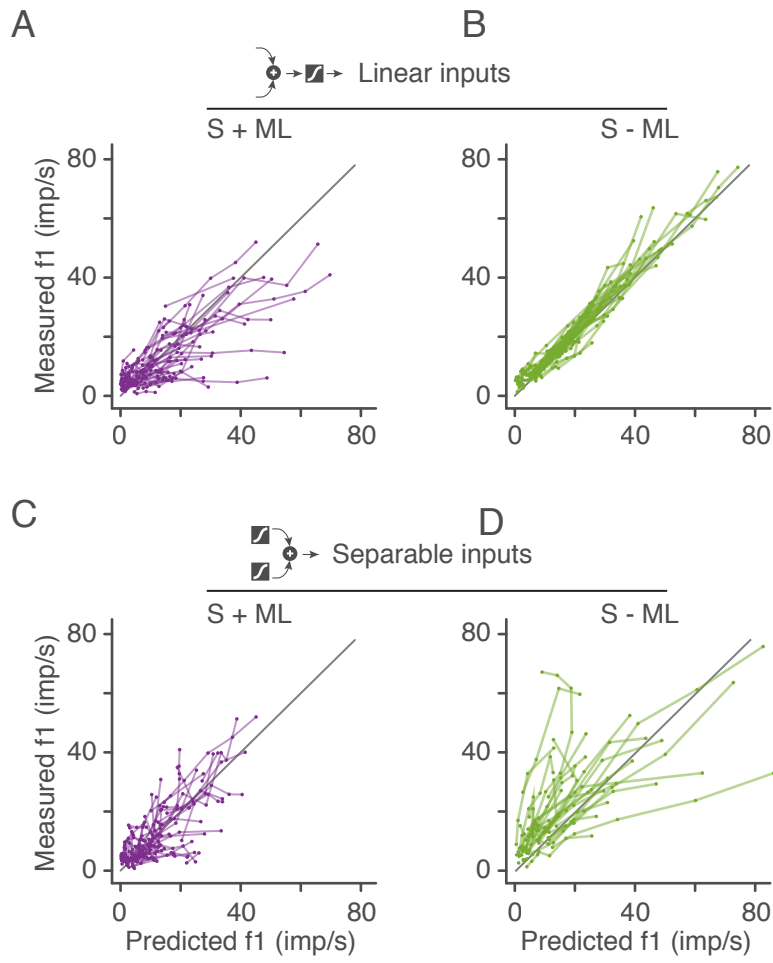
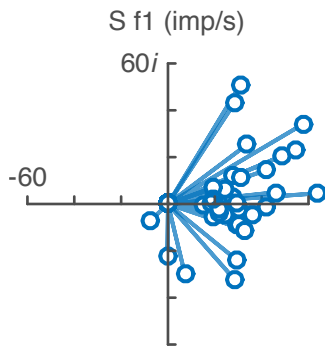
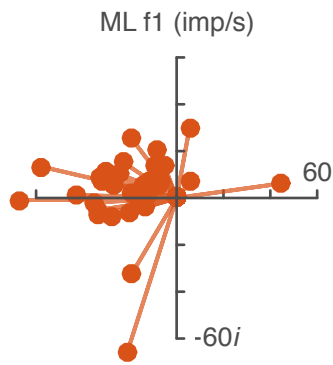


Figure 7

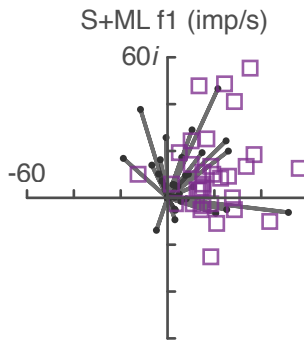
A



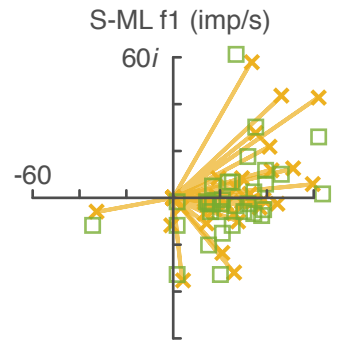
B



C



D



E

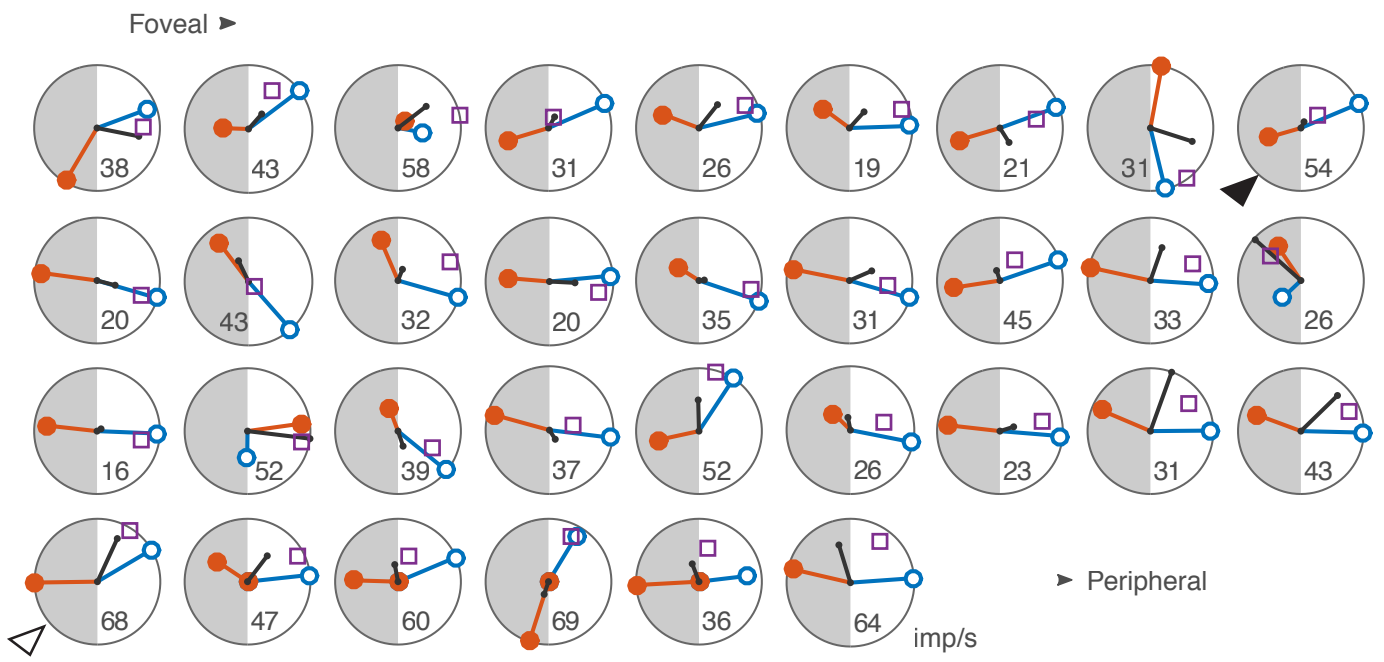


Figure 8

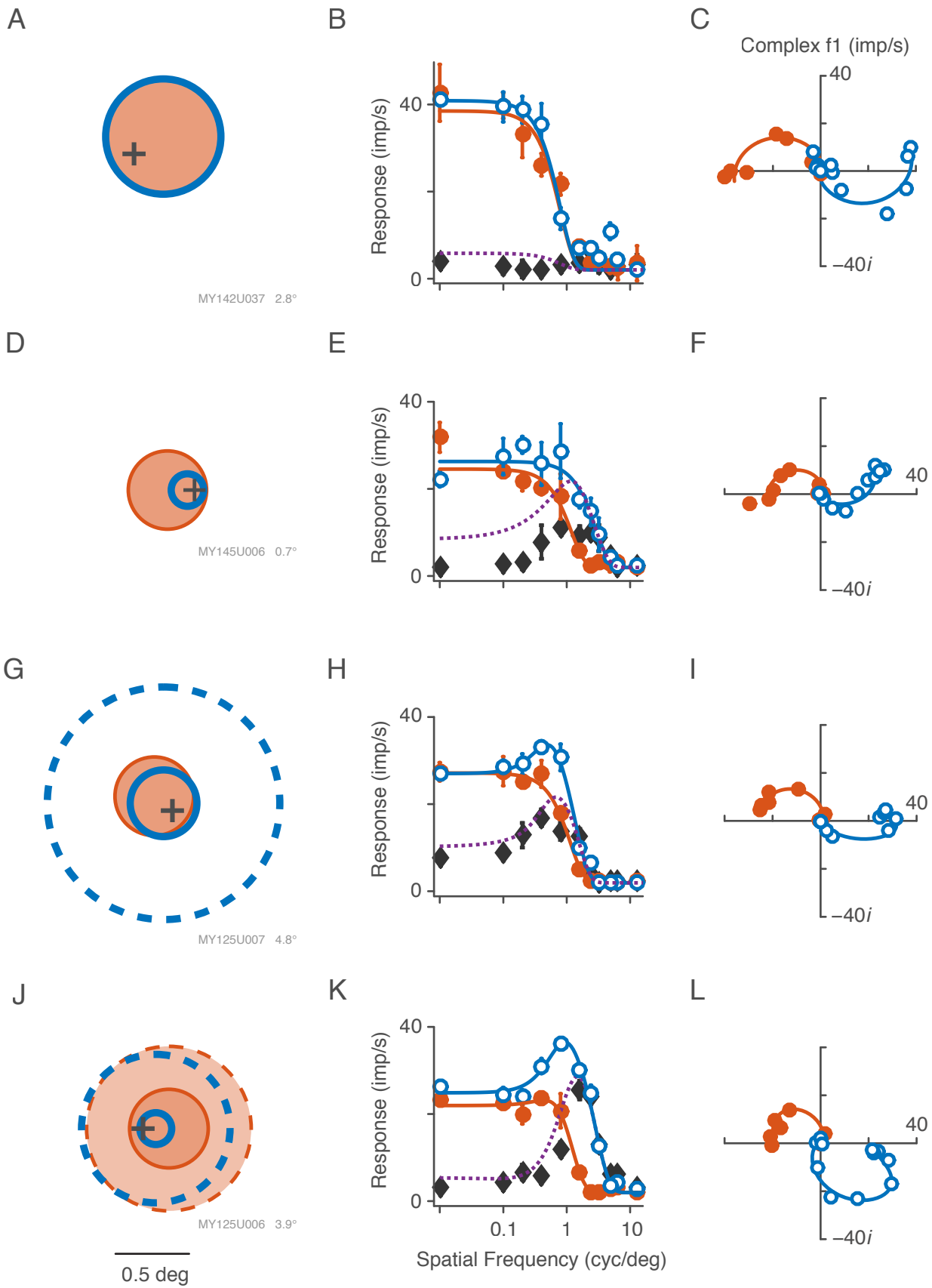


Figure 9

